



ISSN: 2744-6204  
Published 1 October 2020

# Computational Modelling of Glucose Uptake in the Enterocyte

Nima Afshar<sup>1\*</sup>, Soroush Safaei<sup>1</sup>, David P. Nickerson<sup>1</sup>, Peter J. Hunter<sup>1</sup>, and Vinod Suresh<sup>1,2</sup>

<sup>1</sup>Auckland Bioengineering Institute, University of Auckland, New Zealand

<sup>2</sup>Department of Engineering Science, University of Auckland, New Zealand

## ORIGINAL

### Abstract

We describe an implemented model of glucose absorption in the enterocyte, as previously published by Afshar et al. Afshar et al. (2019), The model used mechanistic descriptions of all the responsible transporters and was built in the CellML framework. It was validated against published experimental data and implemented in a modular structure which allows each individual transporter to be edited independently from the other transport protein models. The composite model was then used to study the role of the sodium-glucose cotransporter (SGLT1) and the glucose transporter type 2 (GLUT2), along with the requirement for the existence of the apical Glut2 transporter, especially in the presence of high luminal glucose loads, in order to enhance the absorption. Here we demonstrate the reproduction of the figures in the original paper by using the associated model.

Keywords: PHYSIOME, CellML, OpenCOR, Computational modeling, Glucose uptake

### Curated Model Implementation

<http://doi.org/10.3389>

### Primary Publications

N. Afshar, S. Safaei, D. P. Nickerson, P. Hunter, and V. Suresh. Computational modelling of glucose uptake in the enterocyte. *Frontiers in Physiology*, 10:380, 2019. doi: <http://dx.doi.org/10.3389/fphys.2019.00380>.

## OPEN ACCESS Reproducible Model

*Edited by*

Karin Lundengård

*Curated by*

Anand Rampadarath

*\*Corresponding author*

[nima.afshar@auckland.ac.nz](mailto:nima.afshar@auckland.ac.nz)

*Submitted 30 September  
2020*

*Accepted 1 October 2020*

*Citation*

Afshar et al. (2020)

Computational Modelling of

Glucose Uptake in the

Enterocyte. *Physiome*.

doi: [10.36903/physiome.13034423](https://doi.org/10.36903/physiome.13034423)

## 1 Introduction

In the primary paper, a validated computational model was proposed for explaining glucose uptake from intestinal lumen into epithelial cell. The main goal of this paper is to show that the figures in the primary paper can be reproduced by using the correlated model in the PMR. Results from the model were compared with experimental results from Zheng et al. (Zheng et al., 2012) which studied the glucose uptake on two different cell lines - Caco2 and IEC6 - by using varying concentration of glucose (0.5 - 50 mM). Here we introduce a quick instruction to reproduce each figure in the original paper.

## 2 Model description

We present a mathematical model that includes apical GLUT2 and is parameterised against published experimental data, and was used to study the contributions of SGLT1 and GLUT2 in published cell culture data on glucose uptake (Zheng et al., 2012). The implemented model used mechanistic models of all relevant transporters. In particular, we replaced the Na-Cl co-transporter in the original model with individual models for the anion exchanger 1 (AE1) and Na<sup>+</sup>/H<sup>+</sup> exchanger (NHE3) proteins at the apical membrane and incorporated ENaC and CFTR channels

for apical  $\text{Na}^+$  and  $\text{Cl}^-$  transport. This makes it possible to use the model to study scenarios where the expression and/or function of these transport proteins is altered, for example in gene knockout/mutation studies or in the use of channel inhibitors and agonists. We constructed a mathematical model of the epithelial cell of a small intestine (enterocyte) that incorporates the relevant transport proteins identified in the literature (Barrett and Keely, 2015) and diffusion pathways (figure 1). The membrane localisation and function of these transporters and the source of the original mathematical models are listed in Table 1.

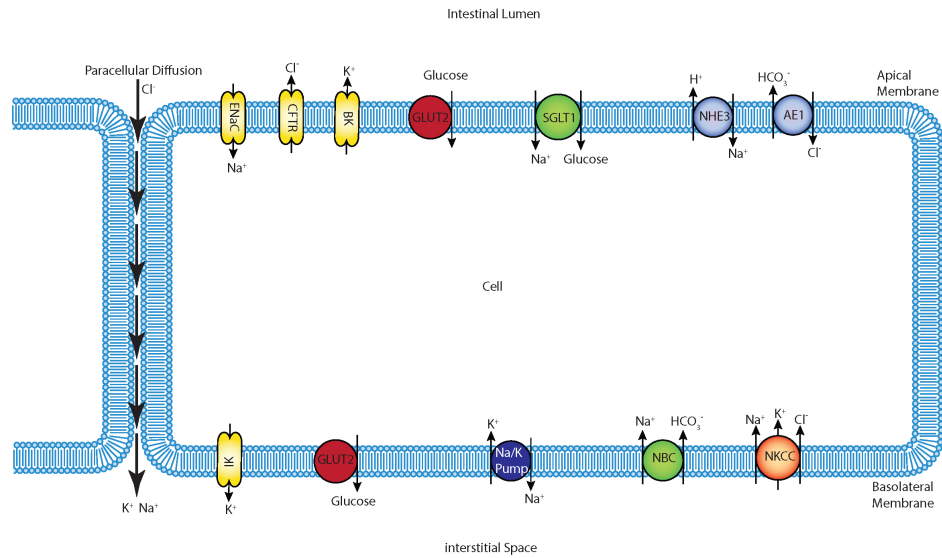


**Figure 1.** Schematic of enterocyte showing the relevant transporters in the apical and basolateral membrane along with the apical (lumen) and basolateral (interstitium) extracellular domains.

The apical (luminal) and basolateral (interstitial) surface of the cell are in contact with distinct extracellular compartments. Transport of substances occurs across the membranes as well as directly between the extracellular compartments across the paracellular junctions. The variables to be solved in the model are chemical species ( $\text{Na}^+$ ,  $\text{K}^+$ ,  $\text{H}^+$ ,  $\text{Cl}^-$ ,  $\text{HCO}_3^-$ , glucose) concentrations in each compartment and the two membrane potentials. Flux balance and electric charge conservation laws yield the governing equations of the model. Water transport is not included and hence we limit ourselves to modelling iso-osmotic transport.

Transporter	Location	Role	Chemical Species	Source of the mathematical model
SGLT1	Apical	Cotransporter	1 Glucose, 2 $\text{Na}^+$	Parent et al. (1992)
NaK ATPase	Basolateral	Exchange Pump	3 $\text{Na}^+$ , 2 $\text{K}^+$	Thorsen et al. (2014)
GLUT2	Apical and Basolateral	Uniporter Protein	Glucose	Pradhan et al. (2013)
NHE3	Apical	Antiporter	1 $\text{Na}^+$ , 1 $\text{H}^+$	Weinstein (1995)
AE1	Apical	Antiporter	1 $\text{Cl}^-$ , 1 $\text{HCO}_3^-$	Weinstein (2000)
BK	Apical	Channel	$\text{K}^+$	Fong et al. (2016)
CFTR	Apical	Channel	$\text{Cl}^-$	Fong et al. (2016)
CLC-2	Basolateral	Channel	$\text{Cl}^-$	Fong et al. (2016)
ENaC	Apical	Channel	$\text{Na}^+$	Fong et al. (2016)
IK	Basolateral	Channel	$\text{K}^+$	Fong et al. (2016)
NBC	Basolateral	Cotransporter	1 $\text{Na}^+$ , 3 $\text{HCO}_3^-$	Østby et al. (2009)
NKCC1	Basolateral	Cotransporter	1 $\text{Na}^+$ , 1 $\text{K}^+$ , 2 $\text{Cl}^-$	Palk et al. (2010)

**Table 1.** List of transporters used in the model along with their locations and roles

The model is implemented in the open source, extensible markup language (XML)-based CellML modelling environment used to represent mathematical models of biology based on ordinary differential and algebraic equations (Cuellar et al., 2003). We adopted a modular, compositional approach to model construction by reusing CellML models of individual transport proteins encoded in an online, curated repository (Physiome Model Repository (PMR, [models.physioimeproject.org](https://models.physioimeproject.org))) to facilitate the sharing of models (Yu et al., 2011). All simulation were run using OpenCOR (Version 0.5) (Garny and Hunter, 2015). All results presented here can be reproduced using the SED-ML or Python scripts noted in the figure captions. In some cases the simulation results are saved to CSV files for plotting using a Python script also noted in the figure caption. We used python 3.6 with the following versions of different libraries: numpy 1.17.4, matplotlib 3.1.2, pandas 0.25.3, scipy 1.3.3.

The original CellML file along with all the codes can be found in the following link in the PMR:

<https://models.physioimeproject.org/workspace/572>

### 3 Model results

#### *Dynamic response to an apical glucose stimulus*

In these simulations, the compositions of the apical and basolateral compartments were identical and held constant (140 mM Na<sup>+</sup>, 5.4 mM K<sup>+</sup>, 103 mM Cl<sup>-</sup>). A time dependant, extracellular glucose stimulus was applied at t = 60 s (Figure 2A). The simulation file Fig02.sedml contains the computational setting for running the model.

#### *Comparison with the Thorsen et. al model (Thorsen et al., 2014)*

In the next step the results from our model were compared to results from Thorsen model under the same condition. Model outputs were normalised against the steady state values of the Thorsen model and are shown in Figure 3. We implemented the Thorsen model in CellML which can be found in the PMR link <sup>1</sup>. All the values in our model are normalised against the corresponding steady-state values in the Thorsen model as described in the python script.

---

<sup>1</sup><https://models.physioimeproject.org/workspace/5b8>

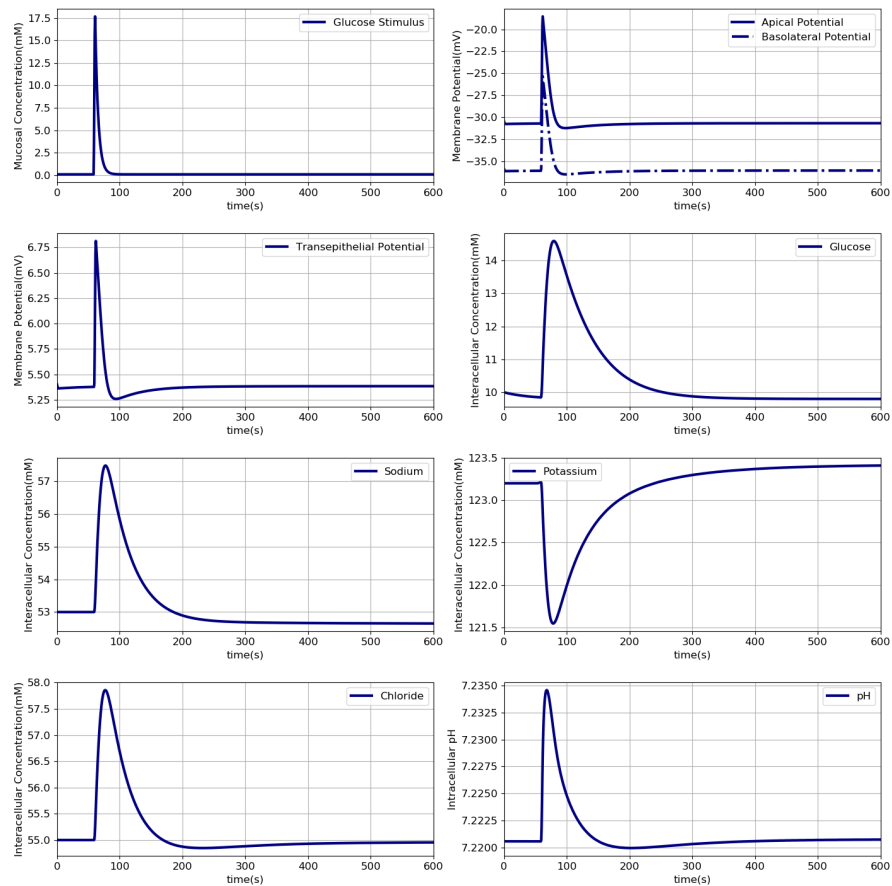


**Figure 2.** Dynamic response of the model to an extracellular glucose stimulus. The stimulus consists of: A - a step increase followed by an exponential decay. B - Apical and basolateral membrane potentials, C - transepithelial potential, D - and intracellular concentrations of glucose, E - sodium, F - potassium, G - chloride and H - pH are shown. The results presented in the figure 2 can be reproduced with the Fig02.py in OpenCOR's python interface

### Comparison against cell culture data

Finally, model predictions were compared against measurements carried out in cell culture studies (Zheng et al., 2012). The experiments used Caco-2 and IEC6 cell lines. While Caco-2 expresses both SGLT1 and GLUT2, IEC6 cells do not express GLUT2. We therefore turned off the expression of GLUT2 in the apical membranes to simulate these cells (in component "Cell\_Concentration",  $\theta_{26}=0$ ). To measure glucose uptake, varying concentrations (0.5 - 50 mM) of glucose were introduced into the apical chamber in a buffer solution with a baseline composition of 130 mM NaCl, 4 mM  $\text{KH}_2\text{PO}_4$ , 1 mM  $\text{CaCl}_2$ . The osmolarity of the buffer was maintained during the measurements by modulating the NaCl content such that if the glucose concentration was  $x$  mM, NaCl concentration was  $130 - x/2$  mM. After exposure to the glucose stimulus for different durations (30 - 600 s), cells were lysed and intracellular glucose and protein concentrations were measured. Since the measurements were reported in nanomole glucose per milligram (mg) protein, the data were converted to concentration units (millimole per litre, mM) by doing the unit conversion from nanomole/ $m^3$  to mM and also multiplying by the cellular protein concentration (mg protein per ml cell volume). The conversion factor  $a$  (protein density) was used as a fitting parameter in a non-linear Generalized Reduced Gradient optimization to match model outputs to the data. The optimization was done using the Microsoft Excel Solver (Microsoft Office 2013) by minimizing the least square error between model predicted and measured intracellular glucose concentration. These results indicate that the model is able to reproduce a range of

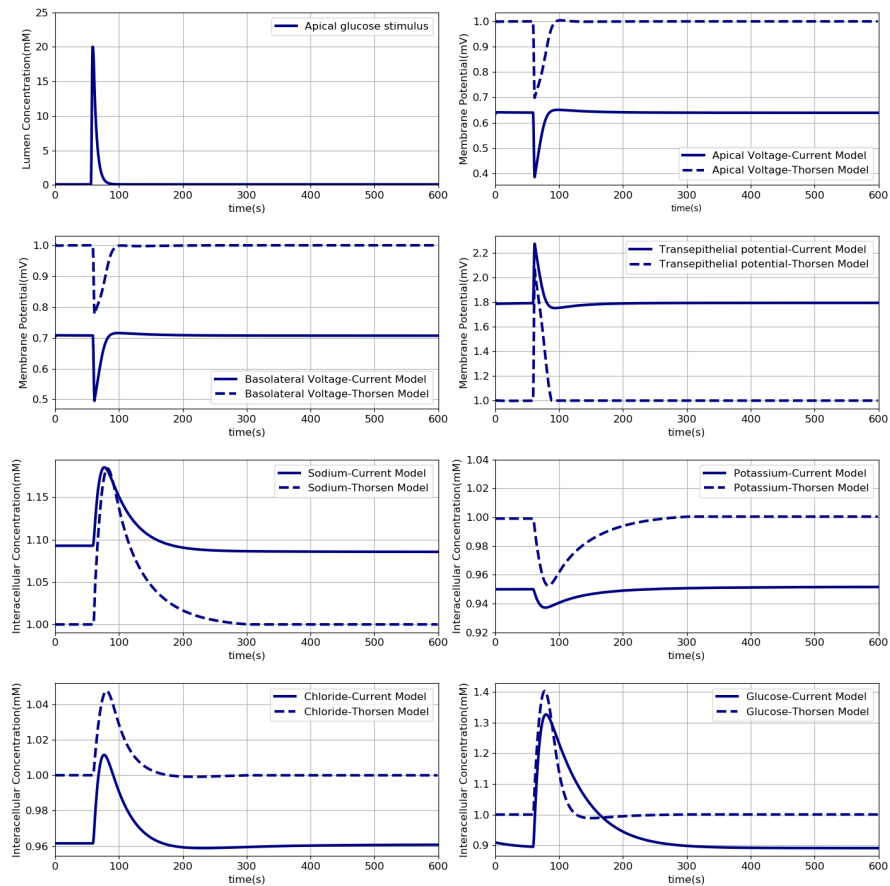


**Figure 3.** Comparison of model responses against the model of Thorsen et al (2014). Each variable has been normalised against the corresponding steady value from the Thorsen model. The results presented in the figure 3 can be reproduced with the Fig03.py script in OpenCOR's python interface and Fig03-plot.py script

independent experimental observations. The volume of the basolateral compartment ( $V_b$ ) was fixed at different multiples ( $m = 0.1, 1, 10$ ) of the cell volume ( $V_c$ ) and also as an infinite bath to generate a range of predictions. This allowed us to account for the uncertainty in the actual volume of the basolateral compartment, we collected a range of model predictions by varying the parameter from small (0.1 times the cell volume) to large (an infinite compartment) values (figure 4).

### *Role of apical GLUT2 in glucose uptake*

In the original study of Zheng et al, the experimental data in Figure 4 were interpreted as indicating the presence of GLUT2-mediated uptake at the apical membrane (Zheng et al., 2012). In figure 5 we investigated whether an alternative explanation was possible whereby SGLT1 expression levels in the model could be tuned to reproduce the same trends in intracellular glucose concentration. In Figure 5, the data for Caco-2 cells at the 600 s time point are compared to the model with varying levels of apical GLUT2 and SGLT1. The baseline model with normal expression of SGLT1 and apical GLUT2 provides a good fit to the data over the full range of apical glucose concentrations (Figure 5A). When apical GLUT2 is turned off (in component "Cell\_Concentration",  $\theta_{26}=0$ ) with no changes in SGLT1 expression (Figure 5B), model predictions of intracellular glucose are low compared to the data for apical glucose concentrations higher than 10 mM. In addition, model predictions saturate after around 20 mM of apical glucose while the data shows an increasing trend. A higher expression of SGLT1 was also examined and can provide a better match to the data in the absence of apical GLUT2. With no apical GLUT2 and 2-fold levels of baseline SGLT1 (Figure 5C) the model

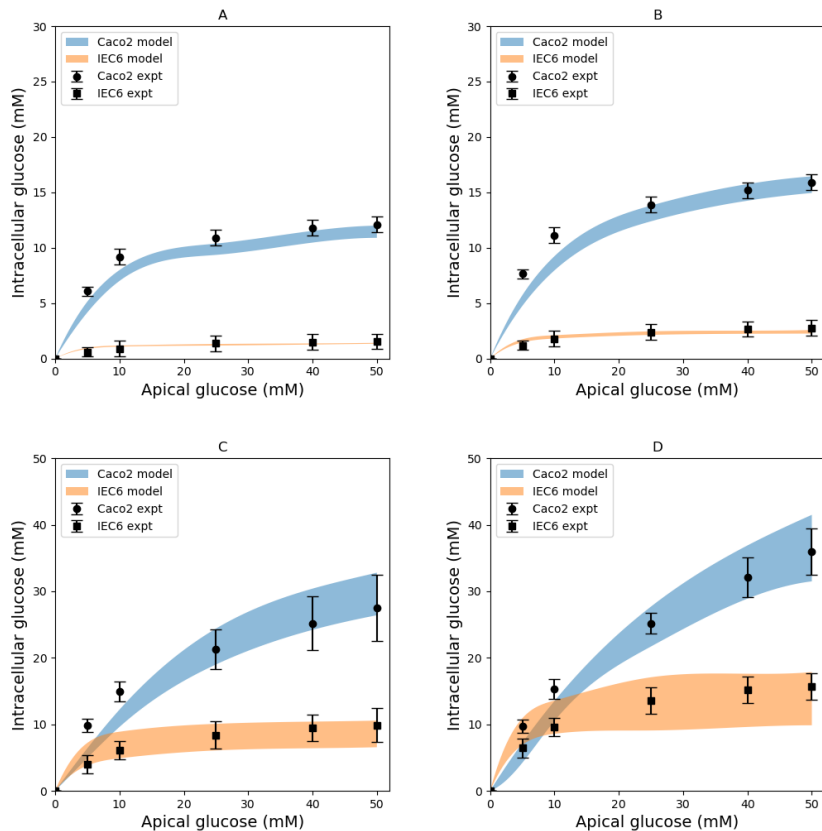


**Figure 4.** Intracellular glucose concentrations for a range of extracellular glucose concentrations in Caco2 and IEC6 cells and exposure times (A: 30 s, B: 60 s, C: 300 s, D: 600 s). Experimental data points and error bars were digitally extracted from Zheng et al (2012). Strips for the model predictions represent the range of values generated by setting  $V_b = mV_c$ ,  $m = 0.1, 1, 10, \infty$ . The results presented in the figure 4 can be reproduced with the Fig04.py script in OpenCOR's python interface and Fig04-plot.py script

overpredicts the data at low apical glucose concentrations (< 10 mM) and underpredicts the data at apical glucose concentrations > 40 mM (in component "SGLT1\_Flux",  $n_{SGLT} \times 2$ ). When SGLT1 levels are increased to 3 times the baseline value (in component "SGLT1\_Flux",  $n_{SGLT} \times 3$ ), the model overpredicts the data over the whole range, except at an apical glucose of 50 mM (Figure 5D)

The contribution of SGLT1 and GLUT2 to the apical glucose flux is shown in Figure 6 following 600 s of exposure to apical glucose. The figure shows SGLT1 flux (where in component "Cell\_Concentration",  $\theta_{26}=0$ ), GLUT2 flux (where in "Cell\_Concentration",  $\theta_6=0$ ) and the total flux which is basically SGLT1 flux + GLUT2 flux. For different glucose loads in the lumen, the concentration of ions needs to be changed as described for figure 4.

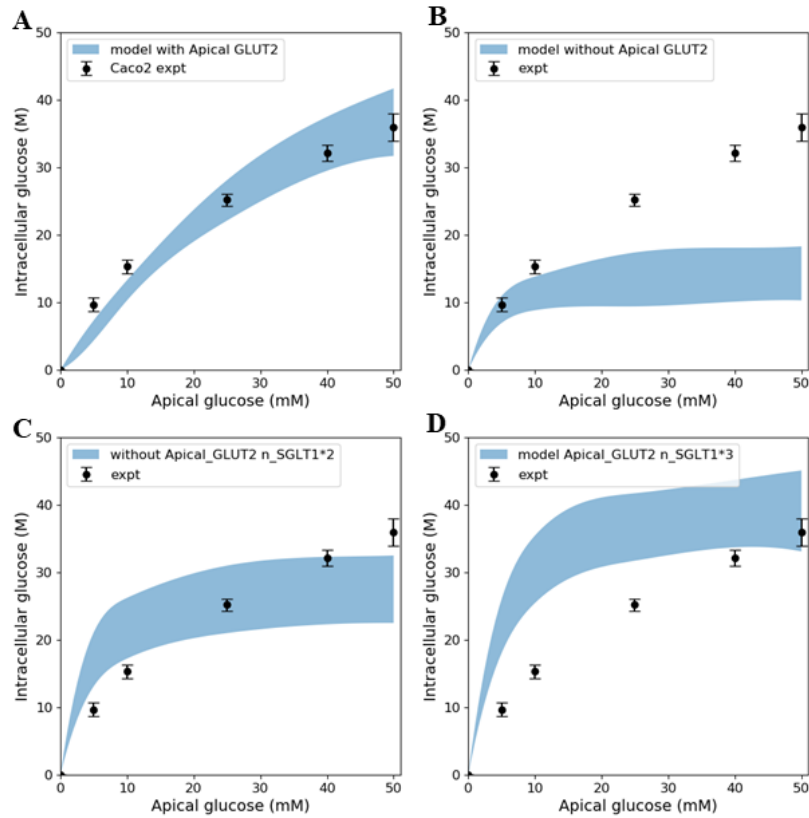


**Figure 5.** Intracellular glucose concentration versus extracellular glucose concentration in Caco2 in the presence/absence of Apical GLUT2 with different numbers of SGLT1 transporter A - Output of model with apical GLUT2 B - Model does not have apical GLUT2 C - Model does not have apical GLUT2 and the number of SGLT1 is doubled D - Model does not have apical GLUT2 and the number of SGLT1 is 3-fold higher. Experimental data points and error bars were digitally extracted from Zheng et al (2012). Strips for the model predictions represent the range of values generated by setting  $V_b = mV_c$ ,  $m = 0.1, 1, 10, \infty$ . The results presented in the figure 5 can be reproduced with the Fig05.py script in OpenCOR's python interface and Fig05-plot.py script

The developed model was then used to study the effect of 3-fold elevated SGLT1 and GLUT2 expression levels on glucose flux into the basolateral compartment. Figure 7 shows the ratio of steady state glucose flux into the basolateral compartment, normalised to the flux at baseline conditions over a range of apical glucose concentrations. In green line the number of SGLT1 protein was multiplied by 3 (in component "SGLT1\_Flux",  $n_{SGLT} \times 3$ ) and in blue line the number of GLUT2 transporter in both membranes was tripled (in component "A\_Glut" and "GLUT2",  $n_{GLUT} \times 3$ ) and in red line both the SGLT1 and GLUT2 protein were increased 3-fold. For different apical glucose concentrations, other ion concentrations should be changed as described for figure 4. All the values for each set were divided by the basolateral flux values from baseline conditions.

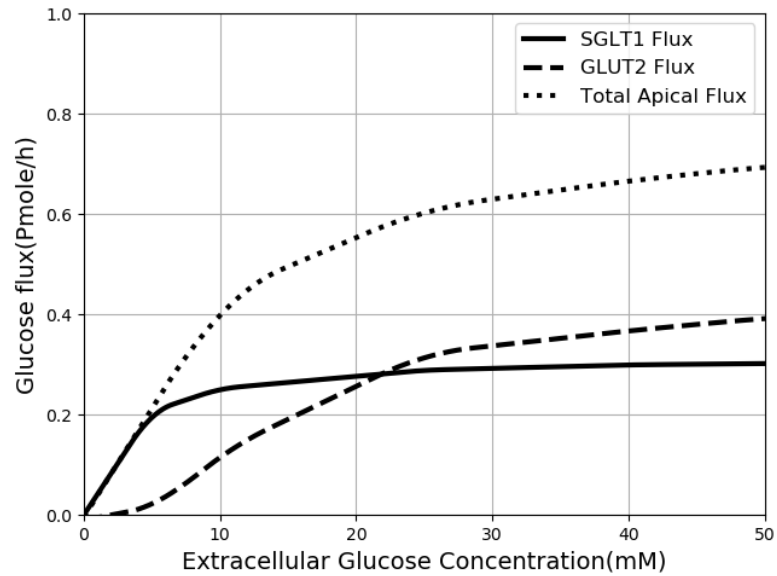


**Figure 6.** Glucose Flux through SGLT1 and GLUT2 in 600 seconds of simulation along with total apical flux of glucose. The results presented in the figure 6 can be reproduced with the Fig06.py script in OpenCOR's python interface and Fig06-plot.py script

We developed a computational model of glucose transport in the enterocyte that includes the full set of relevant transporters. The model is able to reproduce measurements reported in the literature and can be used to answer physiologically relevant questions about glucose uptake rates and mechanisms. In addition, the capabilities of the CellML framework were exploited to compose existing validated models of individual transporters to create the final model, which provides greater confidence in the implementation and facilitates model reuse and sharing.

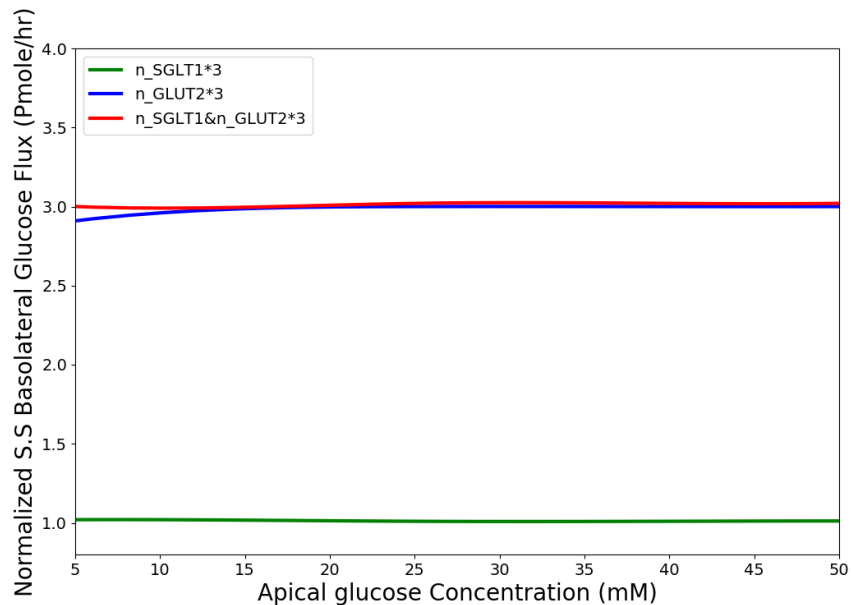


**Figure 7.** Normalised steady state basolateral glucose flux versus different stimulus of glucose in the lumen when number of SGLT1 is 3 fold higher (green), number of GLUT2 is 3 fold higher (blue) and number of both SGLT1 & GLUT2 are 3 fold higher (red). The results presented in the figure 7 can be reproduced with the Fig07.py script in OpenCOR's python interface and Fig07-plot.py script

## 4 Discussion

### Comparison with existing models

Our model differs from the Thorsen et al. model (Thorsen et al., 2014) in some important respects. One of the differences between the two models is in the treatment of sodium and chloride transport at the apical membrane. Thorsen et al postulate electro neutral one-for-one fluxes of these ions to account for the sodium-hydrogen (NHE3) and chloride-bicarbonate (AE1) exchangers and use Goldman-Hodgkin-Katz (GHK) diffusion to model ENaC and CFTR. In contrast, our model takes a more general approach by incorporating the individual transport pathways at the apical membrane (Figure 1). We examined the implications of these modelling choices in Figure 8. Figure 8A shows the ratio of the AE1 flux to NHE3 flux for the simulation conditions of Figure 3. In the Thorsen model this ratio is equal to 1, whereas the ratio lies in the range 7 - 8 in our model. File Fig02.sedml was run in the OpenCOR in order to plot chloride flux through AE1 over sodium flux via NHE3.  $J_{NHE3\_Na}$  and  $J_{AE1\_Cl}$  were plotted and all the data points in AE1 were divided by corresponding value in the NHE3 data set. Cl/Na cotransporter ratio as stated in the paper is equal to 1. Thorsen et al. used sodium and chloride diffusion through both apical and basolateral membrane of the cell. We replaced them with ENaC and CFTR transporters for sodium and chloride flux in the apical membrane respectively. Figure 8B shows the ratio of sodium and chloride flux through transporters in our model to the sodium and chloride flux through diffusion in the Thorsen model.

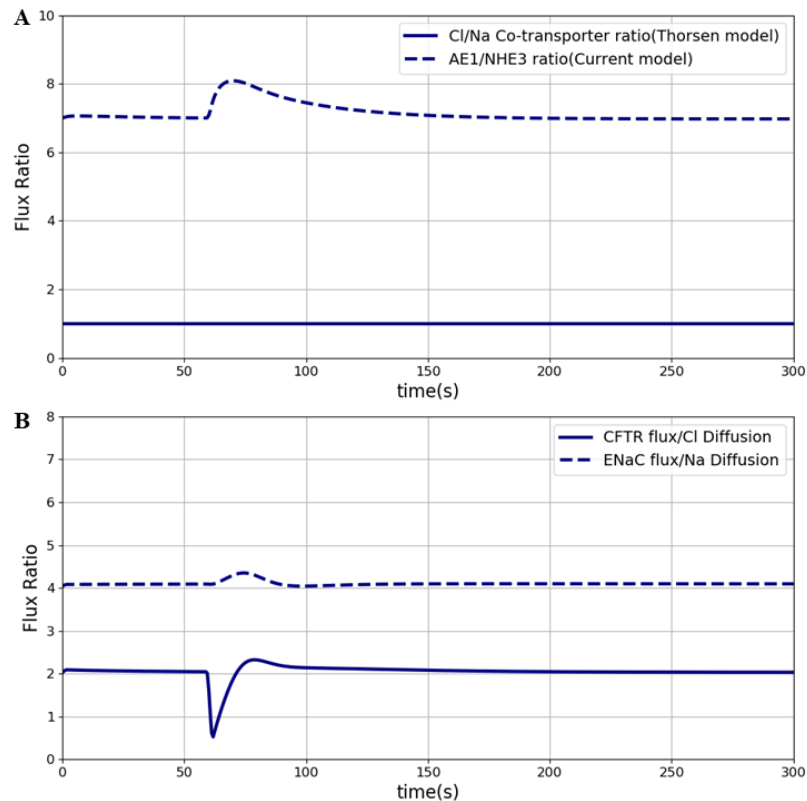


**Figure 8.** Sodium flux and Chloride flux through NHE3 and AE1 compare to NaCl co-transporter flux in the Thorsen model. The results presented in the figure 8 can be reproduced with the Fig08.py script in OpenCOR's python interface and Fig08-plot.py

Figure 9 shows the model output in each cell line separately. They both were plotted at different exposure times which indicates that over a short time (30 and 60 seconds) both the cell lines have tendency to level off. Over a longer time ( $\geq 300$  seconds) IEC6 still has a tendency to be saturated but in Caco2 glucose uptake keeps increasing in higher luminal glucose. Figure 9 is another way to show figure 4 however it does not contain the experimental results by having all the exposure times for specific cell lines in one panel. Once again, strips for the model predictions represent the range of values generated by setting  $V_b = mV_c, m = 0.1, 1, 10, \infty$ . In this paper we described how each graph was plotted in the original paper to make things easier for other scientists in this area to become familiar with the entire process. We also showed that the primary model can be reproduced which may be a useful feature in generating other related models or expanding the current model.

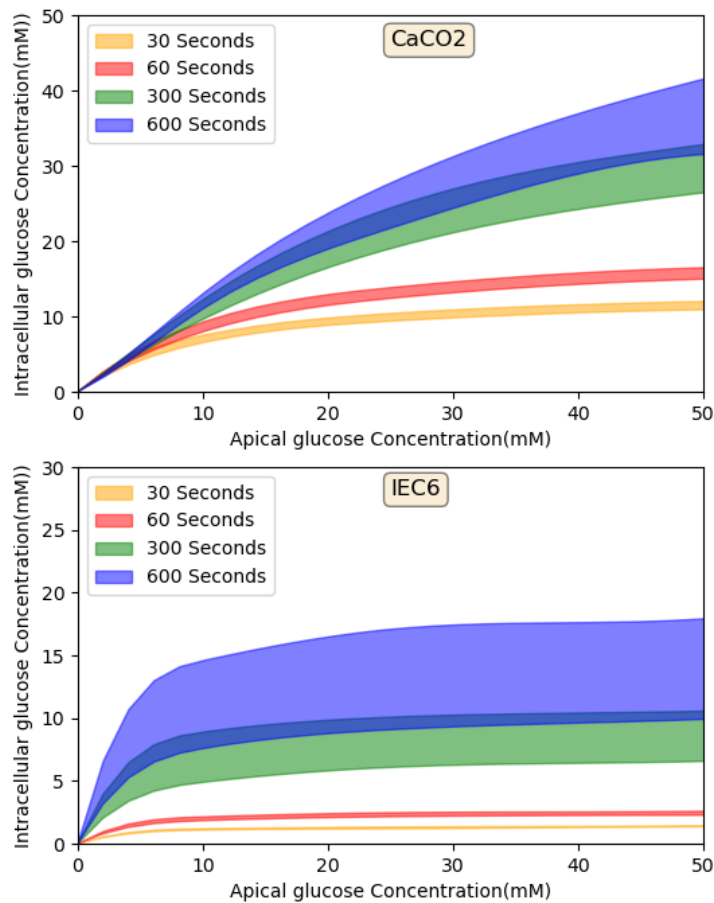


**Figure 9.** Model output - Intracellular glucose concentration versus Extracellular glucose concentration in a) Caco2 cell line and b) IEC6 cell line. The results presented in the figure 8 can be reproduced with the Fig09.py script in OpenCOR's python interface and Fig09-plot.py

## References

- N. Afshar, S. Safaei, D. P. Nickerson, P. Hunter, and V. Suresh. Computational modelling of glucose uptake in the enterocyte. *Frontiers in Physiology*, 10:380, 2019. doi: <http://dx.doi.org/10.3389/fphys.2019.00380>.
- K. E. Barrett and S. J. Keely. Electrolyte secretion and absorption in the small intestine and colon. *Yamada's Textbook of Gastroenterology*, pages 420–449, 2015.
- A. A. Cuellar, C. M. Lloyd, P. F. Nielsen, D. P. Bullivant, D. P. Nickerson, and P. J. Hunter. An overview of cellml 1.1, a biological model description language. *Simulation*, 79(12):740–747, 2003.
- S. Fong, J. A. Chiorini, J. Sneyd, and V. Suresh. Computational modeling of epithelial fluid and ion transport in the parotid duct after transfection of human aquaporin-1. *American Journal of Physiology-Gastrointestinal and Liver Physiology*, 312(2):G153–G163, 2016.
- A. Garny and P. J. Hunter. Opencor: a modular and interoperable approach to computational biology. *Frontiers in physiology*, 6:26, 2015.
- I. Østby, L. Øyehaug, G. T. Einevoll, E. A. Nagelhus, E. Plahte, T. Zeuthen, C. M. Lloyd, O. P. Ottersen, and S. W. Omholt. Astrocytic mechanisms explaining neural-activity-induced shrinkage of extraneuronal space. *PLoS Comput Biol*, 5(1):e1000272, 2009.
- L. Palk, J. Sneyd, T. J. Shuttleworth, D. I. Yule, and E. J. Crampin. A dynamic model of saliva secretion. *Journal of theoretical biology*, 266(4):625–640, 2010.
- L. Parent, S. Supplisson, D. D. Loo, and E. M. Wright. Electrogenic properties of the cloned  $\text{na}^+/\text{glucose}$  cotransporter: ii. a transport model under nonrapid equilibrium conditions. *Journal of Membrane Biology*, 125(1):63–79, 1992.
- R. K. Pradhan, K. C. Vinnakota, D. A. Beard, and R. K. Dash. Carrier-mediated transport through biomembranes. *Transport in Biological Media*, pages 181–212, 2013.
- K. Thorsen, T. Drengstig, and P. Ruoff. Transepithelial glucose transport and  $\text{na}^+/\text{k}^+$  homeostasis in enterocytes: an integrative model. *American Journal of Physiology-Cell Physiology*, 307(4):C320–C337, 2014.
- A. M. Weinstein. A kinetically defined  $\text{na}^+/\text{h}^+$  antiporter within a mathematical model of the rat proximal tubule. *The Journal of general physiology*, 105(5):617–641, 1995.
- A. M. Weinstein. A mathematical model of the outer medullary collecting duct of the rat. *American Journal of Physiology-Renal Physiology*, 279(1):F24–F45, 2000.
- T. Yu, C. M. Lloyd, D. P. Nickerson, M. T. Cooling, A. K. Miller, A. Garny, J. R. Terkildsen, J. Lawson, R. D. Britten, P. J. Hunter, et al. The physiome model repository 2. *Bioinformatics*, 27(5):743–744, 2011.
- Y. Zheng, J. S. Scow, J. A. Duenes, and M. G. Sarr. Mechanisms of glucose uptake in intestinal cell lines: role of  $\text{glut2}$ . *Surgery*, 151(1):13–25, 2012.

**Reproducibility report for:** Computational Modelling of Glucose Uptake in the Enterocyte.

**Submitted to:** *Physiome*

**Manuscript number/identifier:** S000008

**Curation outcome summary:** Successfully reproduced all the figures presented in this manuscript.

**Box 1: Criteria for repeatability and reproducibility**

**■ Model source code provided:**

- Source code: a standard procedural language is used (e.g. MATLAB, Python, C)
  - There are details/documentation on how the source code was compiled
  - There are details on how to run the code in the provided documentation
  - The initial conditions are provided for each of the simulations
  - Details for creating reported graphical results from the simulation results

Source code: a declarative language is used (e.g. SBML, CellML, NeuroML)

- The algorithms used are defined or cited in previous articles
- The algorithm parameters are defined
- Post-processing of the results are described in sufficient detail

**Executable model provided:**

- The model is executable without source (e.g. desktop application, compiled code, online service)
  - There are sufficient details to repeat the required simulation experiments

**■ The model is described mathematically in the article(s):**

- Equations representing the biological system
- There are tables or lists of parameter values
- There are tables or lists of initial conditions
- Machine-readable tables of parameter values
- Machine-readable tables of initial conditions

**The simulation experiments using the model are described mathematically in the article:**

- Integration algorithms used are defined
- Stochastic algorithms used are defined
- Random number generator algorithms used are defined
- Parameter fitting algorithms are defined
- The paper indicates how the algorithms yield the desired output

**Box 2: Criteria for accessibility**

- Model/source code is available at a public repository or researcher's web site
  - Prohibitive license provided
  - Permissive license provided
  - Open-source license provided
- All initial conditions and parameters are provided
- All simulation experiments are fully defined (events listed, collection times and measurements specified, algorithms provided, simulator specified, etc.)

**Box 3: Rules for Credible practice of Modeling and Simulation<sup>a</sup>**

<sup>a</sup>Model credibility is assessed using the Interagency Modeling and Analysis Group conformance rubric:  
<https://www.imagwiki.nibib.nih.gov/content/10-simple-rules-conformance-rubric>

- Define context clearly: Extensive
- Use appropriate data: Extensive
- Evaluate within context: Extensive
- List limitations explicitly: Insufficient
- Use version control: Extensive
- Document adequately: Extensive
- Conform to standards: Insufficient

**Box 4: Evaluation**

- Model and its simulations could be repeated using provided declarative or procedural code
- Model and its simulations could be reproduced



**Summary comments:** Model and source code are available in the associated OMEX archive. This was used in our attempt to reproduce the results presented in the paper. We successfully ran the SED-ML files to reproduce Figure 2 - Figure 9 as presented in this manuscript.

Anand K. Rampadarath<sup>1</sup>, PhD  
Curator  
Center for Reproducible Biomedical Modeling

David P. Nickerson, PhD  
Curation Service Director  
Center for Reproducible Biomedical Modeling

Auckland Bioengineering Institute,  
University of Auckland

---

<sup>1</sup>Email: [a.rampadarath@auckland.ac.nz](mailto:a.rampadarath@auckland.ac.nz)